Journal Pre-proof

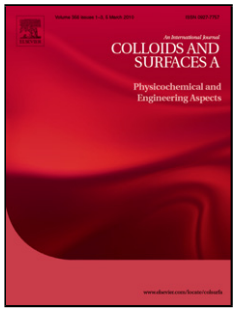

A pH-sensitive drug delivery system based on folic acid-targeted HBP-modified mesoporous silica nanoparticles for cancer therapy

Yan Li, Shuai Wang, Fang Xiang Song, Li Zhang, Wei Yang, Hong Xia Wang, Qian Lin Chen

PII: S0927-7757(20)30062-5

DOI: https://doi.org/10.1016/j.colsurfa.2020.124470

Reference: COLSUA 124470

To appear in: *Colloids and Surfaces A: Physicochemical and Engineering Aspects*

Received Date: 6 December 2019

Revised Date: 14 January 2020

Accepted Date: 14 January 2020

Please cite this article as: Li Y, Wang S, Song FX, Zhang L, Yang W, Wang HX, Chen QL, A pH-sensitive drug delivery system based on folic acid-targeted HBP-modified mesoporous silica nanoparticles for cancer therapy, *Colloids and Surfaces A: Physicochemical and Engineering Aspects* (2020), doi: https://doi.org/10.1016/j.colsurfa.2020.124470

A pH-sensitive drug delivery system based on folic acid-targeted HBP-modified mesoporous silica nanoparticles for cancer therapy

Yan Li[1,4], Shuai Wang[1,4], Fang Xiang Song[2], Li Zhang[2], Wei Yang[1,4] and Hong Xia Wang[2], Qian Lin Chen[3]*

[1]School of Pharmacy, Guizhou University, Guiyang 550025, China

[2]School of Chemistry and Chemical Engineering，Guizhou University，Guiyang 550025, China

[3]Institute of Advanced Technology, Guizhou University, Guiyang 550025, China

[4]Guizhou Pharmaceutical Engineering Laboratory, Guiyang 550025, China

*Corresponding author: qlchen@gzu.edu.cn

Graphical Abstract

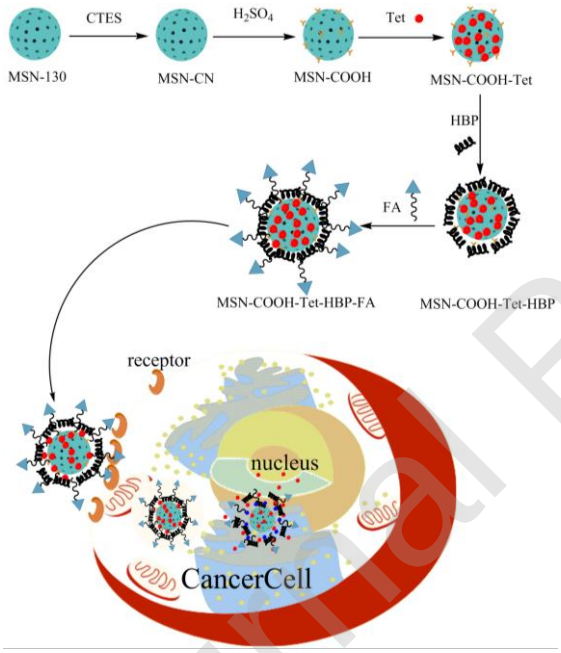

Mesoporous silica nanoparticles with folic acid (MSN-COOH-Tet-HBP-FA) are able to mediate targeting and have a pH stimulation response character, and therefore have been successfully synthesized as vectors for antitumor drug delivery. The model drug is tetrandrine (Tet). The chemical structure and properties of these NPs were characterized through systematic characterization analyses. Their drug loading capacity was significantly improved through carboxy modification (26.86 % in max), and they exhibited pH-dependent drug release profiles("zero pre-release" within 20 hours in a normal physiological environment). In vitro cytotoxicity and cell uptake of the as-synthesized NPs in Hela and A549 cells were also evaluated, and exhibited high cytotoxicity and cell-targeted uptake capacity. It was concluded that MSN-COOH-Tet-HBP-FA could be used as a promising drug delivery system for cancer therapy.

Abstract

Mesoporous silica nanoparticles with folic acid (MSN-COOH-Tet-HBP-FA) are able to mediate targeting and have a pH stimulation response character, and therefore have been successfully synthesized as vectors for antitumor drug delivery. The model drug is tetrandrine (Tet). The chemical structure and properties of these NPs were characterized through systematic characterization analyses. Their drug loading capacity was significantly improved through carboxy modification (26.86 % in max), and they exhibited pH-dependent drug release profiles("zero pre-release" within 20 hours in a normal physiological environment). In vitro cytotoxicity and cell uptake of the as-synthesized NPs in Hela and A549 cells were also evaluated, and exhibited high cytotoxicity and cell-targeted uptake capacity. It was concluded that MSN-COOH-Tet-HBP-FA could be used as a promising drug delivery system for cancer therapy.

Keywords： Mesoporous silica, Tetrandrine, Folic acid, Cancer therapy

1. Introduction

Cancer is currently considered to be a leading factor that threatens human lives, and chemotherapy remains one of the most common methods used for cancer treatment[1,2]. However, traditional drugs are nonspecific and cannot discriminate cancer cells and normal cells, which not only limits the accumulation of drugs in tumor cells, but also leads to systemic toxicity and adverse side effects[3,4]. In order to improve the efficacy of chemotherapy, many studies have been devoted to the development of tumor-targeted nanocarriers, which can be used to control the delivery of antitumor drugs[5-7]. Using the enhanced permeation and retention (EPR) effects, researchers have developed multiple nanocarrier platforms, including liposomes[8,9], polymer nanoparticles[10], nano-micelles[11,12], and dendrimers[13,14], which are used to delivery anticancer drugs into tumor tissues. However, the EPR effect is not efficient enough to eradicate the side effects of cytotoxic drugs and to exert the anticancer therapy selectively in cancer cells[15]. In order to enhance the targeting and tumoral uptake ability, the external surface of nanocarrier is often modified with various ligands, which can significantly enhance the interaction between the cancer cells and the nanocarriers[16-18]. Targeted agents typically include antibodies (such as monoclonal antibodies) [19,20], peptides (such as Arg-Gly-Asp (RGD)) [21-23], and small molecule compounds (such as folic acid) [24-26].

Over the past few decades, the use of a controlled drug delivery systems(DDS) has been widely explored widely in anti-cancer fields[27]. The ideal drug delivery system should be stable and able to hold the unreleased loaded drugs through the circulation in the bloodstream or in normal tissues. Upon reaching and accumulating in tumor tissues by passive and active targeting, it will be taken up by cancer cells, and the drugs should be released rapidly in response to the local environment. Due to its responsiveness and adaptability, stimulation-responsive polymers have been widely studied and developed in the fields of environmental monitoring, electronics, photonics, controlled drug release and medical imaging. In recent years, mesoporous silica nanomaterials (MSN) have attracted much attention due to their unique advantages, such as high specific surface area and large pore volume, homogeneous controllable particle size and well-defined surface property for modification[28-31]. Moreover, the studies have indicated that mesoporous silica materials possess good biocompatibility and biodegradability[32,33]. These features make mesoporous silica materials as drug carriers.

Stimulated-responsive terminated amino hyperbranched polymer (HBP) has a large number of terminal amino groups and branches. They have attracted a lot of attention in recent years due to their unique spherical cavity-like topology, low solution viscosity and good solubility. The structural characteristics, functionalization and pH responsiveness of HBP provides a powerful platform for the practical application of a pH-based triggered HBP system[34]. Folic acid (FA), a water-soluble B vitamin that is stable and nonimmunogenic, binds selectively to the folate receptor (FR)[35-37]. The FR, known as a glycophosphatidylinositol-linked cell surface receptor, is a high affinity membrane folate-binding glycoprotein[38,39]. As the FR is generally overexpressed on the surface of a variety of human cancer cells and has a high affinity to FA binding[40-42], a wide range of FA-conjugated drug delivery carriers have been thoroughly investigated[43,44]. Tetrandrine(Tet) is a kind of dibenzylquinoline alkaloid isolated from traditional Chinese medicine, which has a long history of application in the clinical treatment of various diseases in China. It has been reported as a cellular autophagy agonist[45] and a lysosomal inhibitor[46], and has potent anti-tumor effects when used alone or in combination with other drugs[45-47]. And it was explained that tetrandrine is a hydrophobic drug, and its bioavailability can be improved through the delivery of nano-carrier materials, which can further exert its antitumor effect. Moreover, tetrandrine has a relatively low toxicity to humans even when administered at high doses, thus we choose tetrandrine as a model drug.

In this paper, mesoporous silica nanoparticles with a particle size of 130 nm were prepared and the adsorption capacity of the antitumor drug tetrandrine was increased by surface carboxy functionalization, and then the surface of the material was modified by terminated amino hyperbranched polymer and folic acid target agents (MSN-COOH-Tet-HBP-FA) (Scheme 1). The engineered materials can be efficiently captured by cancer cells through receptor-mediated endocytosis and then rapidly release the loaded anti-tumor drugs at an acidic pH. Several functions were built into the multifunctional MSNs in order to

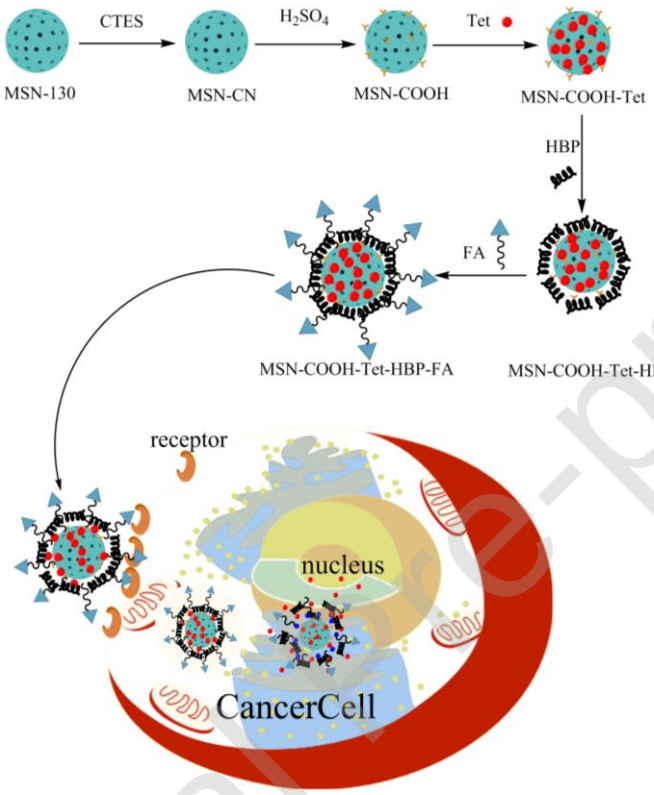

Scheme 1 Schematic illustration showing the possible formation of MSN-COOH-Tet-HBP-FA and the subsequent drug loading and delivery process

deliver drugs in an optimal fashion: i) functionalized with the carboxyl groups on the nanoparticles to graft the terminated amino hyperbranched polymer molecule and increase the loading capacity of tetrandrine ; ii) active tumor targeting folic acid ligands were attached to the surface of the nanoparticles; iii) graft the terminated amino hyperbranched polymers were grafted on the surface of the nanoparticles to block the mesoporous channel; iv) pH-triggered drugs to be released within acidic intracellular compartments such as the endosome and lysosome. The design of drug carriers with these functions can reduce the cytotoxicity to healthy cells and improve the delivery of antitumor drugs.

2. Material and methods

2.1. Materials

Tetraethylorthosilicate (TEOS; AR, Tianjin, China), diethylenetriamine (DETA; AR, Shanghai, China), cetyltrimethyl ammonium bromide (CTAB; AR, Tianjin, China), 3-aminopropyl triethoxysilane (APTES), methyl acrylate (MA; AR, Shanghai, China), 2-cyanoethyltriethoxysilane (CTES; AR, Shanghai, China), vitriolic acid (H_2SO_4; AR, Chongqing, China), methylbenzene (AR, Chongqing, China), hydrochloric acid (HCl, 36-38%, Chongqin, China), N-hydroxysuccinimide (NHS; AR, Shanghai, China), ammonia solution ($NH_3 \cdot H_2O$; AR, Chengdu, China), folic acid (FA; AR, Shanghai, China), 3-dimethylaminopropyl)-3-ethyl carbodiimide (EDC; AR, Shanghai, China), fluorescein isothiocyanate (FITC; AR, Shanghai, China), N,N-dimethylformamide (DMF; AR, Shanghai, China), ethanol and methanol (EtOH, MeOH; AR, Tianjin, China)，2-(N-morpholine)ethanesulfonic acid buffer solution (MES; pH 5), phosphate-buffered saline (PBS; pH 4.5 and pH 7.4), and tetrandrine (Tet) were purchased from Aladdin (Shanghai, China) and used without further purification. All water used was deionized.

2.2. Synthesis of Terminated Amino Hyperbranched Polymer

The terminated amino hyperbranched polymer was prepared according to the previous study[48]. Diethylene triamine (52 ml, 0.5 mol) was added in a 250-ml three-neck round-bottomed glass flask equipped with a constant-voltage dropping funnel, a thermometer and a nitrogen inlet tube. The reaction mixture was stirred with a heat-up magnetic agitator and cooled with an ice bath, while the solution of methyl acrylate (43 ml, 0.5 mol) in methanol (100 ml) was added dropwise into the flask. Then the mixture was removed from the ice bath and left stirring for a further 4 h at room temperature. The light yellow AB_2 type monomer was synthesized and then the mixture was transferred to an eggplant-shaped flask for an automatic rotary vacuum evaporator. After removing the methanol under low pressure, the temperature was raised to 150℃ using an oil bath, and left for 4 h until the yellowish viscid scale terminated amino hyperbranched polymer was obtained.

2.3. Synthesis of Carboxyl Functionalized Mesoporous Silica Nanoparticles

2.3.1. Synthesis of Mesoporous Silica Nanoparticles

CTAB (0.78 g) was dissolved in a mixture of distilled H_2O (220 mL) and methanol (80 mL) under vigorous stirring (1200 rpm)，while the pH value was adjusted to 11.24 with ammonium hydroxide. The mixture reaction was heated to 80 ℃. TEOS (5 mL) was then added dropwise, stirred for 3 h, and aged for another 3 h. The resulting solid was filtered and washed with excessive distilled H_2O and MeOH,

respectively. Finally, the sample was dried under vacuum to yield the as-synthesized nanoparticles. In order to remove surfactant template (CTAB) from the mesopores of the nanoparticle, the as-synthesized nanoparticle was extracted with a mixture of ethanol (100 mL) and concentrated HCl (10 mL). The substance was called MSN-130.

2.3.2. Synthesis of Carboxyl Functionalized Mesoporous Silica Nanoparticles

Briefly, 500 mg MSN-130 was evenly dispersed in 40 mL dry toluene and bath sonicated for 30 min. Then, 1.5 mL of CTES was added, the mixture was stirred for 15 h at 100 ℃ (800 rpm), and the resulting solid was isolated and washed with dry toluene. The resulting solid was dried under a vacuum at 60 ℃. The substance was called MSN-CN.

Then, 400 mg of MSN-CN was dispersed into 40 mL of ethanol, and 30 mL of dilute sulfuric acid (15 mL of concentrated sulfuric acid added to 15 mL of deionized water) was added. The mixture was stirred for 5 h at 90 ℃ (800 rpm), and the resulting solid was isolated and washed with dry toluene. The resulting solid was dried under a vacuum at 40 ℃. The substance was called MSN-COOH.

2.3.3. HBP Encapsulation of Carboxyl Functionalized Mesoporous Silica Nanoparticles

HBP (1.5 g) was suspended in distilled H_2O (10 mL), followed by adjusting the solution pH to 5~5.5 with 2-(N-morpholino) ethanesulfonic acid (MES) buffer solution (pH 5). MSN-COOH (80 mg) was added to the solution. 1-ethyl-3-(3-dimethylaminopropyl) carbodiimide (40 mg) and N-hydroxysuccinimide (40 mg) were then dissolved in the mixture at room temperature under magnetic stirring for 16 h. The resulting solid was filtered and washed with distilled H_2O and ethanol, and dried under vacuum at 40 ℃ for 24 h to obtain the HBP-encapsulated mesoporous silica nanoparticles, which were called MSN-COOH-HBP.

2.3.4. Conjugation of FA to HBP-Encapsulated Mesoporous Silica Nanoparticles

At room temperature, 2.3 mg FA, 1 mg EDC and 1.5 mg NHS were added to 10 mL PBS buffer solution, and stirred for 15 h (stirring speed 800 rpm). Then 10 mg MSN-COOH-HBP was added, stirred for 24 h, centrifuged and washed with distilled H_2O and ethanol three times. It was dried under vacuum at 40℃ to obtain the final product(MSN-COOH-HBP-FA).

2.4. Drug Loading

MSN-COOH (100 mg) was added to MeOH solution (30 mL) containing Tet (50 mg). After the mixture solution was stirred for 48 h at the speed of 500 rpm in the dark, it was sonicated to maximize the nanoparticle dispersion. Tet-loaded MSN-COOH was obtained by centrifugation at 8000 rpm for 4 min. The loading percentage of Tet in MSN-COOH was estimated through the UV-Vis 6100s absorption measurements by subtracting the amount of Tet in the collected supernatant from the total amount of Tet added. The loading capacity of Tet is calculated according to the formula[49]. The solid was dried under a vacuum at 35 ℃, and named MSN-COOH-Tet.

$$wt.\% = \left[\frac{m_1 - CV}{m_2 + (m_1 - CV)} \right] \times 100\% \quad (1)$$

m_1: the initial mass of Tet, mg;

m_2: mesoporous adsorbent added into MeOH solution, mg;

C: Tet concentration of the supernatant solution, mg/mL;

V: the volume of the supernatant solution, mL.

2.5. Synthesis of FA-Targeted Carboxyl Functionalized Mesoporous Silica Nanoparticles

According to the reported literature[50,51], the folic acid and HBP encapsulation of drug-loaded mesoporous silica nanoparticles was carried out by a one-pot method. The process is as follows:

HBP (1.5 g) was suspended in distilled H_2O (10 mL), followed by adjusting the solution pH to 5~5.5 with 2-(N-morpholino) ethanesulfonic acid (MES) buffer solution (pH 5). MSN-COOH-Tet (80 mg) was added to the solution. N-hydroxysuccinimide (40 mg) and 1-ethyl-3-(3-dimethylaminopropyl) carbodiimide (40 mg) were then dissolved in the mixture at room temperature under magnetic stirring for 16 h. After that, EDC (40 mg) and NHS (40 mg) were added again, followed by 50 mg of folic acid, and stirred for another 24 h. The resulting solid was filtered and washed with H_2O and ethanol, and dried under vacuum at 40 ℃ for 24 h to obtain the HBP encapsulation of carboxyl functionalized mesoporous silica nanoparticles called MSN-COOH-Tet-HBP-FA.

2.6. Fluorescent Labeling

Firstly, 20 mg fluorescein isothiocyanate (FITC) and 0.1 mL 3-aminopropyl triethoxysilane (APTES) were added to 10 mL N, N-dimethyl formamide solution, stirred at 25 ℃ for 4 h. The sample frozen collection was called FITC-APTES.

MSN-COOH (25 mg) and MSN-COOH-Tet-HBP-FA (25 mg) were added to 20 mL ethanol solution, respectively, followed by 0.2 mL of the above prepared FITC-APTES solution, and tehn stirred at 25 ℃ for 16 h. Fluorescent labeled nanomaterials[52] were obtained by centrifugation. The samples are recorded as MSN-COOH-FITC and MSN-COOH-Tet-HBP-FA-FITC, respectively.

2.7. Drug Release

To determine the kinetics of Tet release from the nanoparticles, each drug-loaded sample was carried out in two different buffer solutions (pH 4.5 or 7.4).

The MSN-COOH-Tet and MSN-COOH-Tet-HBP-FA suspensions (3 mL, 1.67 mg mL^{-1}) were dialyzed against phosphate buffer (10 mm phosphate, 50 mL) at 37 °C under different pH conditions(pH 7.4 and pH 4.5). Subsequently, 3 mL of PBS at the different pH values was added into the dialysis bags. Simultaneously, 3 mL of fluid was taken out and 3 mL fresh PBS was immediately added into the flask. UV-6100 was used for wavelength detection absorbance under 280 nm. The accumulated concentration was calculated for each moment:

$$C_C = C_t + \frac{v}{V}\sum_{0}^{t-1} C_t \tag{2}$$

2.8. Cell Assay in Vitro

2.8.1. Cell Cytotoxicity Assay in Vitro

The cytotoxicity of MSN-COOH-Tet-HBP-FA, MSN-COOH, MSN-COOH-Tet and free Tet were evaluated by the MTT assay on A549 cells and Hela cells. The cells were seeded into a 96-well plate at a density of 5×10^3 cells per well in a complete DMEM medium (200 μL) supplemented with 10% calf serum, 1% penicillin, and 1% streptomycin, and then incubated in humidified 5% CO_2 atmosphere at 37 °C for 24 h. The culture medium was then replaced with fresh culture medium (200 μL) containing Tet-loaded MSN at different Tet doses(15.5 μg/mL, 62.5 μg/mL and 250 μg/mL)）. The cells were further incubated for 48 h, and were then washed three times with PBS, and 100 μL of MTT solution (0.5 mg/mL)

was slowly injected into each well and incubated for 4 h. The relative cell viability compared to control wells containing medium without nanoparticles was calculated by [A]test/[A]control, where [A]test and [A]control are the average absorbance of the test and control samples, respectively.

2.8.2. Cell Uptake Assay

Cellular uptake of nanoparticles was observed using a confocal laser scanning microscopys (CLSM). HeLa and A549 cells were seeded in confocal dishes at a concentration of 1 x 10^4. After 24 h, the medium was removed, washed once with PBS, and then medium containing MSN-COOH-Tet-HBP-FA and MSN-COOH of 62.5 ug/mL was added, and then the cells were cultured at 37 ℃, 5 % CO_2 for 12 h. The medium was removed, washed there times with PBS, and incubated with 500 μL of lysosomal marker (Lyso-Tracker Red, 75 nM) for 2 h. The liquid was removed, and the cells were washed three times with PBS. Fixed cells were treated with 3.7% formaldehyde solution, and nuclei were stained with 57 nM DAPI for 15 min, washed again with PBS, and 50% glycerol was added as a mounting solution. Finally, the cells were observed under a confocal laser scanning microscopys (CLSM, LEICA TCS SP8).

2.9. Characterizations

^{1}H NMR spectra were recorded on a Bruker BBFO-400 spectrometer. Dynamic light scattering (DLS) and zeta potential experiments were performed at 25 °C using a Malvern Zetasizer NanoZS instrument. The powder X-ray diffraction (XRD) patterns were recorded using a Rigaku D/Max 2400 diffractometer with a Cu Ka radiation. Fourier transform infrared (FT-IR) spectra were obtained with a Nicolet iS50 spectrophotometer using KBr pellets. The Brunauer-Emmett-Teller (BET) surface area and average pore volume of the synthesized mesoporous silica materials were measured by a Micromeritics ASAP 2020 analyzer at 77 K. Transmission electron microscopy (TEM) images of the samples were taken using a FEi G20 electron microscope operating at 200 kV. The morphological features of samples were investigated by scanning electron microscopy (SEM) on a JEOL-JSM-7500F electron microscope operating at 20 kV, coupled with an EDS micro-analyzer. UV absorbance spectra were obtained with a Mapada UV-6100s spectrophotometer. Thermogravimetric analysis (TGA) was conducted in air on an STA 449C Jupiter® thermal analyzer. The samples were heated from 30 ℃ to 1000 ℃ at a heating rate of 10 ℃/min in air.

3. Results and Discussion

3.1. Preparation and Characterization of Multifunctional MSN

The synthesis of HBP was monitored by FT-IR and ^{1}H NMR. FT-IR spectra of the terminated amino hyperbranched polymer is shown in Figure 1. It was found that the absorptions were at 1466.4 cm^{-1} and 3280 cm^{-1}, corresponding to the $–CH_2–$ bend and the N–H stretch of the primary amino groups and the imino groups, respectively. The absorption at 1643.9 cm^{-1} is characteristic of the C=O stretch in amide bonds (–CONH–). The possible structure of the terminated amino hyperbranched polymer was also confirmed by ^{1}H-NMR spectroscopy. The peak at 2.58 ppm is attributed to protons corresponding to a, b, c, f, j, k and l of HBP. The peak at 2.35 ppm was attributed to protons corresponding to d and i of HBP. The peak at 2.73 ppm was attributed to the corresponding proton of g of HBP. The peak at 3.23 ppm was attributed to the corresponding proton of e of HBP. The peak at 3.28 ppm is attributed to the proton corresponding to h of HBP[48]. All the analyses confirm the successful synthesis of HBP.

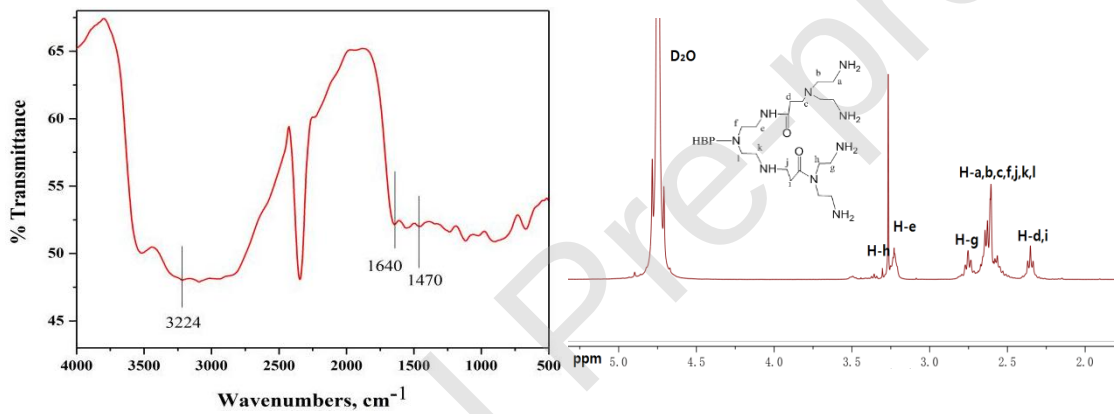

Fig. 1 FTIR spectra and ^{1}H-NMR of terminated amino hyperbranched polymer

Figures 2 shows the scanning electron microscopy (SEM), particle size distribution, and X-ray energy-dispersive spectroscopy (EDS) images of the prepared samples. It can be seen from the SEM diagram that the prepared material is spherical nanoparticles with regular morphology, good dispersion and narrow particle size distribution. The average particle sizes of MSN-130, MSN-COOH-HBP and MSN-COOH-Tet-HBP-FA were 130±16.5 nm, 182±17.9 nm, and 194±21.1 nm, respectively. When the nanoparticles were modified with HBP and FA, the particle size obviously increases, indicating successful grafting of functionalized groups. In addition, it can be seen that N elements appear in the energy spectra of MSN-COOH-HBP and MSN-COOH-Tet-HBP-FA, with percentages of 1.6% and 7.8%, respectively, indicating successful grafting of the terminated amino hyperbranched polymer and tetrandrine.

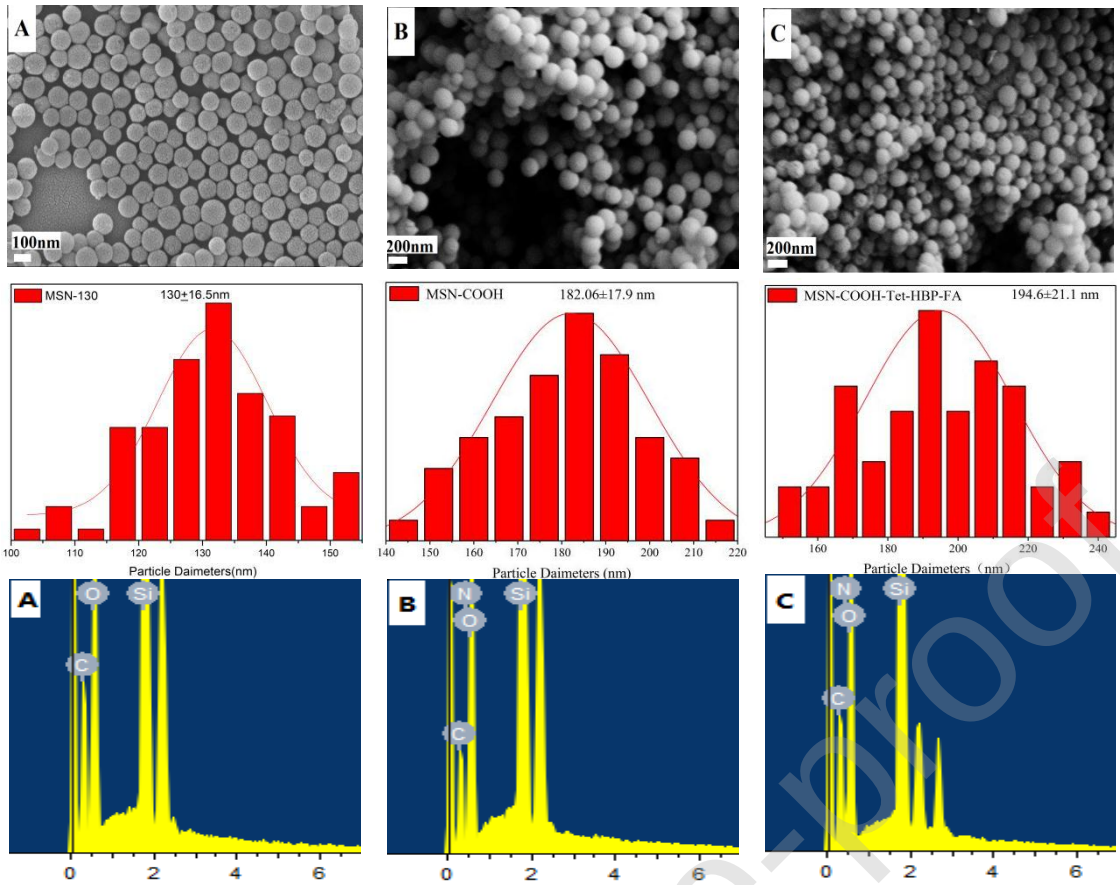

Fig.2 SEM and EDS analysis of MSN-130 (A), MSN-COOH-HBP (B) and MSN-COOH-Tet-HBP-FA (C)

As seen from Figure 3, MSN-130 was uniform spherical nanoparticles, and the mesochannels throughout the entire particle could be seen clearly. The mesopore arrays on the nanoparticles cannot be clearly observed after the introduction of the carboxyl groups and HBP, due to the masking of the polymers. In addition, the nitrogen adsorption and desorption isotherms of all samples were type IV isotherms with hysteresis loops according to the IUPAC classification (Figure 4A). At the low pressure stage ($0 < p/p^0 < 0.4$), the amount of adsorption increases rapidly with the increase of relative pressure, forming a steep step. This is due to capillary condensation of the N_2 molecules adsorbed by the

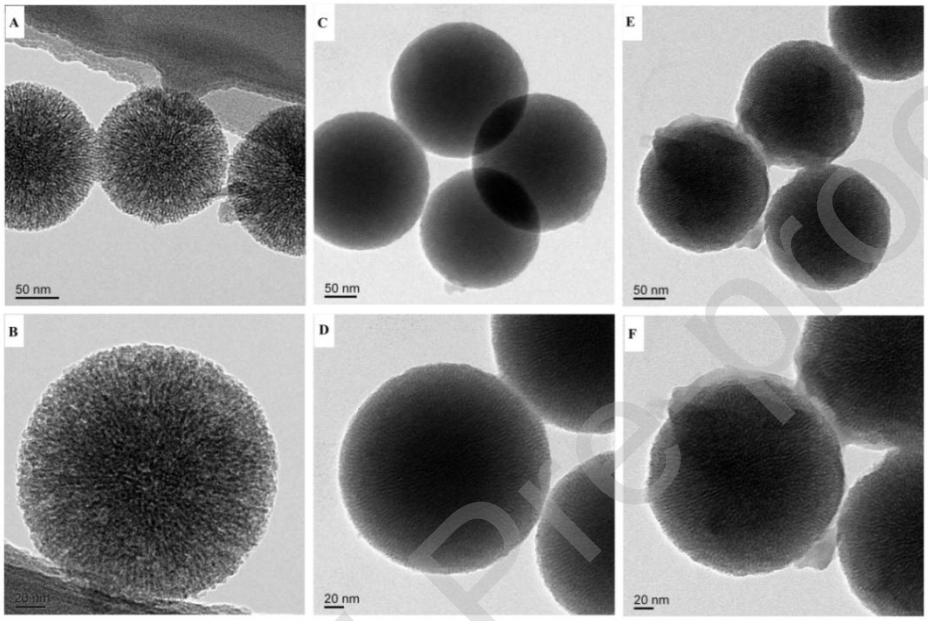

mesoporous sample, which causes the adsorption amount to rise sharply, indicating the existence of mesoporous structure. At the relative pressure $p/p^0 > 0.4$, the N_2 molecules began to adsorb on the outer surface of the mesoporous material, and the curve became relatively flat. A sudden jump appeared at the relative pressure $p/p^0=0.95$. MSN-130 and MSN-COOH exhibited *H4* hysteresis loops, while MSN-COOH-HBP exhibited *H3* hysteresis loops. This indicates that the pore structure of the three materials is irregular, reflecting the flat slit structure or the wedge structure[45].

Fig. 3 TEM images of MSN-130 (A, B), MSN-130-COOH (C, D) and MSN-130-COOH-Tet-HBP-FA (E, F)

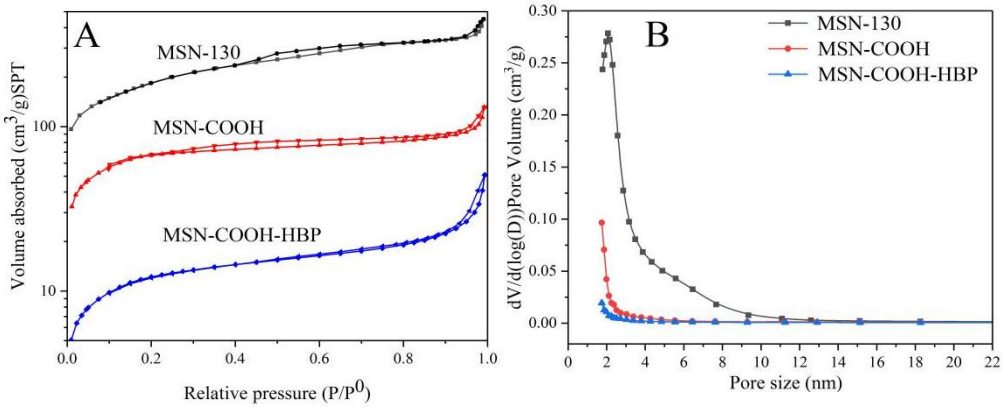

Fig. 4 The nitrogen adsorption-desorption isotherms (A) and pore size distributions (B) of samples MSN-130, MSN-130-COOH and MSN-130-COOH-HBP

Brunauer-Emmett-Teller (BET) and Barrett-Joyner-Halenda (BJH) analyses were used to determine the surface area and pore size of different nanoparticles. As depicted in Figure 4A and Table 1, the BET surface areas of nanoparticles decreased from 786.44 m^2g^{-1} to 254.12 m^2g^{-1} to 46.97 m^2g^{-1} when anchored with carboxyl groups and HBP. Correspondingly, the BJH pore sizes of nanoparticles also changed from 2.060 nm to 1.744 nm to 1.745 nm. These results suggested that the mesopores were successfully capped carboxyl groups and HBP. The pore diameter of MSN-COOH is reduced compared with that of MSN-130, while the pore diameter of BJH of MSN-COOH and MSN-COO-HBP is almost unchanged, indicating that HBP may be grafted to the material surface.

Table 1 Specific surface area, pore volume and pore size of MSN

Sample	Specific surface area (S_{BET}) (m^2 g^{-1})	Pore volume (V_p) (cm^3g^{-1})	BJH adsorption pore
MSN-130	786.44	0.278	2.06
MSN-COOH	254.12	0.189	1.744
MSN-COOH-HBP	46.97	0.069	1.745

The samples were further characterized by FT-IR. As shown in Figure 5A, stretching vibration peaks of the $–CH_2$ of surfactant CTAB were observed at 2810 cm^{-1} and 2930 cm^{-1} in the FT-IR spectrum of MSN-130/CTAB, whereas they were not found in MSN-130, indicating that the template agent was nearly removed. In Figure 5Bd, the bands at 1400 cm^{-1} are attributed to the stretching vibration peaks of C-N. Thus, the characteristic peaks appearing at 1673 cm^{-1} (amide I belt) and 1511 cm^{-1} (amide II belt) are the absorption vibration peaks of CO-NH, which are the absorption peaks of the amide group obtained

by condensation of the amino group on HBPs with the carboxyl group on folic acid, In addition, the band at 1071 cm^{-1} is assigned to the vibration of C-O-C of tetrandrine in Figure 5Ac, whereas, in Figure 5Bc, d, 1071 cm^{-1} is the coincidence peak of the asymmetric stretching vibration absorption peak of Si-O-Si in mesoporous silica and the C-O-C absorption peak generated by Tet. Simultaneously, the characteristic peaks appearing at 1619 cm^{-1}, 1552 cm^{-1} and 1511 cm^{-1} are the stretching vibration peaks of the benzene ring skeleton in Tet, indicating the successful loading of the antitumor drug tetrandrine.

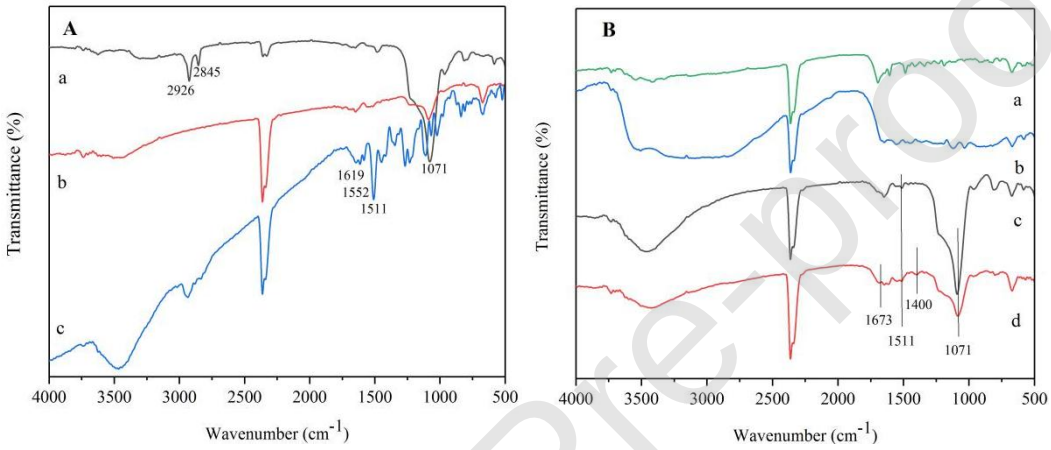

Fig. 5 Infrared characterization of samples A：MSN-130/CTAB (a), MSN-130 (b) and Tet(c); B: FA (a), HBP (b), MSN-COOH-Tet (c) and MSN-COOH-Tet-HBP-FA (d)

Small-angle and wide-angle X-ray diffraction were carried out in order to investigate the regularity of the mesopores. As shown in Figure 6A, small angle X-ray diffraction shows that both MSN-COOH and MSN-COOH-HBP have diffraction peaks at 2θ=2°, indicating that there is an ordered pore structure in the nanomaterials[53]. Furthermore, the intensities of the peaks of MSN-COOH-HBP only changed slightly after being modified with HBP, which showed that HBP functionalization did not influence the ordering of the pore structure. Figure 6B shows the wide-angle X-ray diffraction pattern of the material. Both materials have an distinct broad peak at 15-28°, which is the characteristic peak of typical amorphous silica[54].

Thermogravimetric analysis (TGA) further confirmed the successful surface functionalization of the materials. In Figure 7, the weight loss of the sample MSN-130 at 30-150 ℃ is caused by the adsorption

of water on the surface of the nanoparticles[55]. Afterwards, the percentage weight loss of MSN-130 was about 7.54% at 200-800℃, which was largely due to the removal of silicone groups on the surface of particles. MSN-COOH and MSN-COOH-HBP had a weight loss of 19.92% (H2) and 30.62% (H3) at 200-800℃,which was due to the decomposition of the organic functionalized molecules -COOH and HBP, indicating that functional molecules were successfully immobilized onto the surface of the nanoparticles[56].

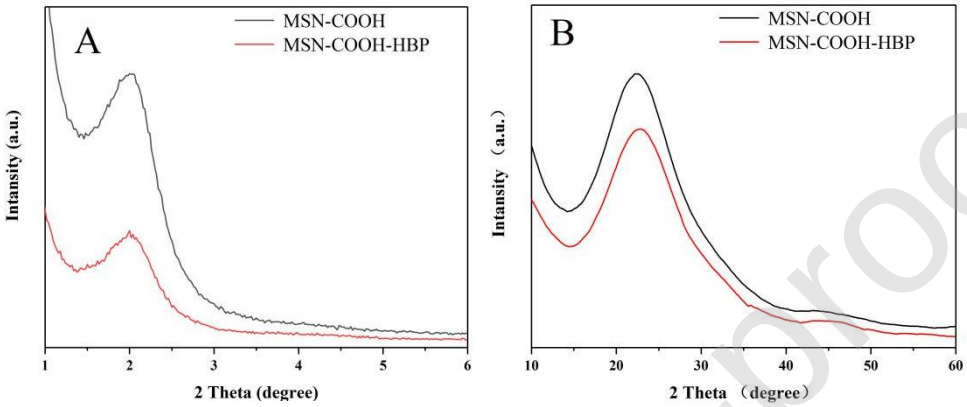

Fig. 6 XRD analysis of the small angle (A) and wide angle (B) of the samples

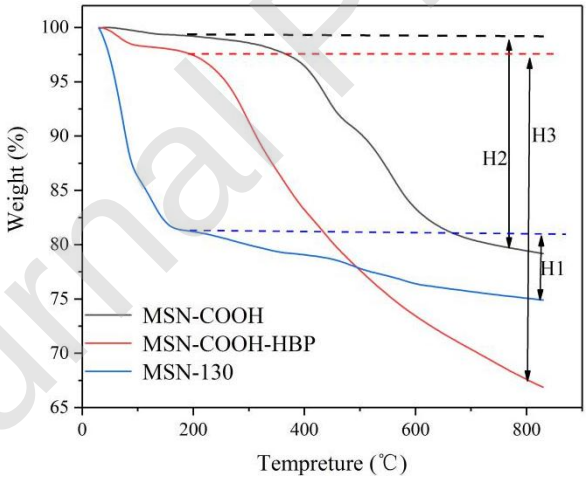

Fig. 7 Thermogravimetric curves of MSN-130, MSN-COOH and MSN-COOH-HBP

Zeta potential experiments and dynamic light scattering (DLS) further confirmed the successful surface functionalization of MSN. Figure 8A shows the Zeta potential diagrams of MSN-130, MSN-COOH and MSN-COOH-HBP. The zeta potential of MSN-130 decreased from -18.10 mV to -22.59 mV, which was caused by the increasing negative charges on the surface of the materials, indicating that carboxyl functionalization was successfully anchored. The Zeta potential of

MSN-COOH-HBP increased to 44.18 mV due to the introduction of a large number of polyaminobranched chains (positive charge) in HBP grafting, indicating that HBP was successfully grafted. In addition, dynamic light scattering (DLS) detection was used to investigate the regular hydrodynamic diameter of HBP on the surface of nanoparticles and the particle size changes at different pH values. In Figure 8B, with the increase of acidity (decreased pH), the particle size of MSN-COOH-HBP decreased from 229 nm to 187 nm, suggesting that HBP will undergo a gradual decomposition process in an acidic environment, which leads to a smaller particle size[57].

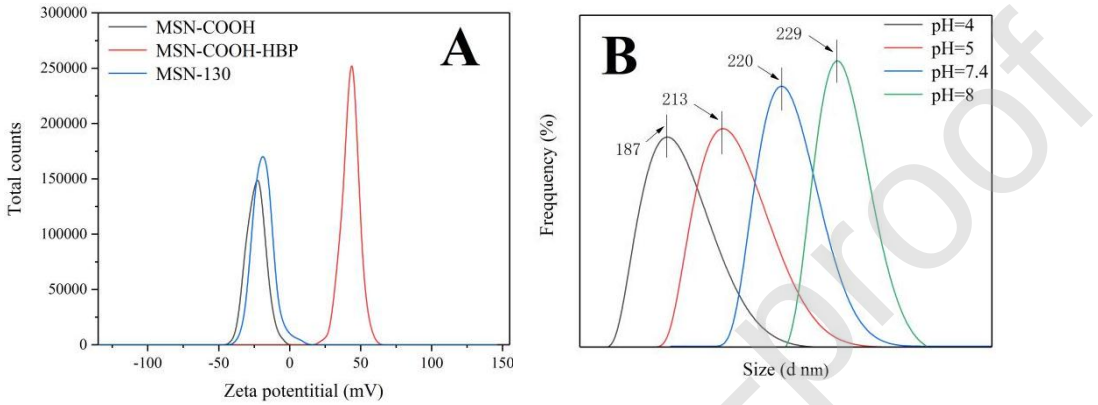

Fig. 8 Zeta potential distribution of MSN-130, MSN-COOH and MSN-COOH-HBP(A), and size distribution of MSN-COOH-HBP at different pH values(B)

The surface functionalization of MSN was further confirmed by XPS analysis (Figure 9, Table 2). In figure 9A, the peaks at 103.73 eV, 155.44 eV, 285.36 eV, 398.99 eV and 531.78 eV are the binding energy of Si 2p, Si 2s, O 1s, N 1s and C 1s of MSN-COOH-HBP samples, respectively, and no N 1s peaks appear in MSN-130, indicating that HBP was successfully grafted on the surface of MSN-130. In Figure 9B, N 1s can be divided into three distinct peaks, N-C (C-N-C) (399.132 eV), O=CN (399.679 eV), and N-H (400.122 eV), indicating the presence of the amino chains in HBP. From the high resolution spectrum of C in figure 9C, a C 1s peak was observed at around 288.944 eV(O-C=O), 286.601 eV(C=O), 285.700 eV(C-O), 284.950 eV(C- N), 284.332 eV(C-C) and 284.313 eV(C-Si), where the presence of C-Si is the cyanation of CTES (silane coupling agent), and O-C=O is assigned to the carboxyl group. The O 1s peaks consist of a SiO_2 peak (284.7 eV), O=C peak (533.177 eV) and C-O peak (531.966 eV)

(Figure 9D). The above analysis indicates a successful carboxylation of -CN and the successful grafting of HBP onto the surface of the nanoparticles.

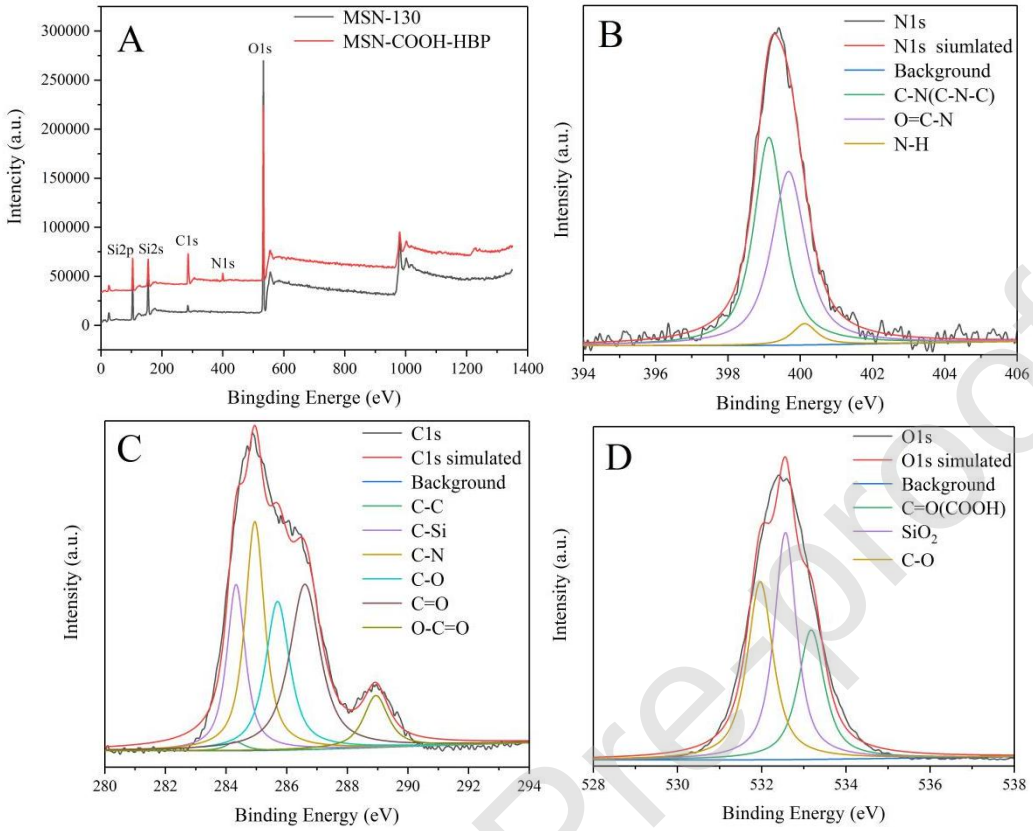

Fig. 9 XPS spectrum of the MSN sample. (A) MSN-130 and MSN-COOH-HBP; (B) N1s of MSN-COOH-HBP; (C) C1s of MSN-COOH-HBP; (D) O1s of MSN-COOH-HBP

3.2. Drug Loading and Release Studies

Drug loading and releasing behavior are the most important characteristics of drug delivery systems[58,59]. Herein, tetrandrine was used as model drug and loaded into MSN-COOH-Tet. Tetrandrine is a kind of dibenzylquinoline alkaloid isolated from traditional Chinese medicine, and the carboxyl and silanol groups of the material can interact with the Tet through hydrogen bonds, thereby increasing its loading capacity. Tetrandrine is typically loaded into the inner channels and surfaces of nanoparticles by diffusion and electrostatic attraction[45]. The drug-loading property of MSN nanocomposites was calculated to be 26.86%, and the Tet loading content was 367.2 ug Tet per mg of nanoparticles.

Figure 10 shows the cumulative release curves of Tet from the nano drug delivery system in simulated physiological environment (PBS buffer, pH 7.4) and tumor tissue acidic environment (PBS buffer, pH 4.5). Both nanoparticles exhibited the typical sustained release behavior. It can be seen from the experimental results that MSN-COOH-Tet has a faster release rate at both pH values, and the maximum release can reach 80% within 72 h before HBP encapsulation and FA targeted modification. Whereas the release of the MSN-COOH-Tet-HBP-FA system was only 30% in 72 h, indicating that the HBP encapsulation improved the controlled release capacity of the drug delivery system. Simultaneously, Tet release from MSN-COOH-Tet-HBP-FA complexes was significantly increased at lower pH values, enabling zero pre-release within 20 hours, which was mainly due to the packaging effect of hyperbranched polymer HBP. Meanwhile, HBP undergoes a process of gradual decomposition (see figure 8) in an acidic environment, which accelerated the drug release rate and achieved the controlled release of the drug, indicating that the modification of HBP gives an obvious pH-dependent drug release behavior. The high drug loading capacity and the pH-dependent sustained release manner suggested that MSN-COOH-Tet-HBP-FA was a promising carrier for anticancer drugs.

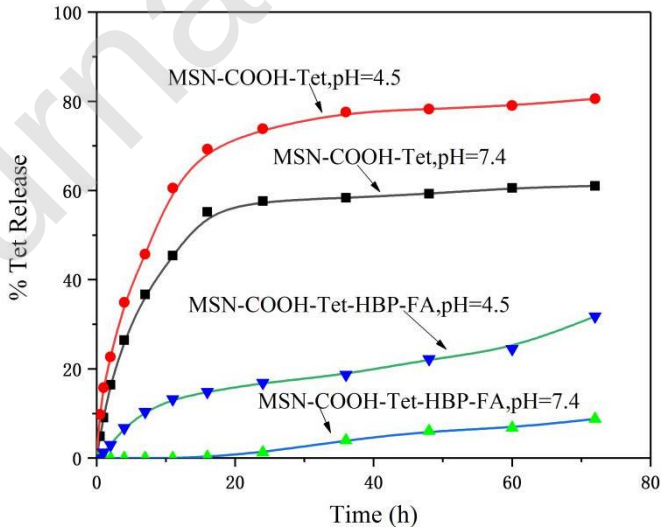

Fig. 10 Release behavior of Tet from MSN-COOH-Tet and MSN-COOH-Tet-HBP-FA nanoparticles

3.3. In Vitro Cytotoxicity Assay

Investigation into the cytotoxicity of drug delivery vehicles is necessary for a drug delivery system. The in vitro cell cytotoxicity of MSN-COOH-TET-HBP-FA against A549 cells and hela cells was assessed by the MTT method. As can be seen from Figure 11, the free antitumor drug Tet was less toxic to Hela cells and A549 cells at a low concentration, but showed significant dose-dependent cytotoxicity with increasing drug concentrations. It was explained that Tet is a kind of hydrophobic drug, which needs to be enriched to a certain concentration to be able to exert its anti-tumor efficacy. As figure 11 shows, MSN-COOH is of moderate toxicity to Hela and A549 cells. After loading the drug, MSN-COOH-Tet showed significant dose-dependent cytotoxicity to both cells. It was explained that the way in which free Tet enters the cells depends primarily on passive diffusion, while the hydrophobicity of Tet resulted in less cytotoxicity at low concentrations in a short period of time. The drug was released from MSN-COOH-Tet under acidic conditions, which increased the cytotoxicity. While the drug was loaded and encapsulated (MSN-COOH-Tet-HBP-FA), cytotoxicity was greatly reduced relative to MSN-COOH-Tet, which may be due to the fact that the drug molecule is blocked by HBP in the material, resulting in a lower release within 48 h. These results indicated that the MSN-COOH-Tet-HBP-FA nanoparticles are more suitable as vehicles for drug delivery.

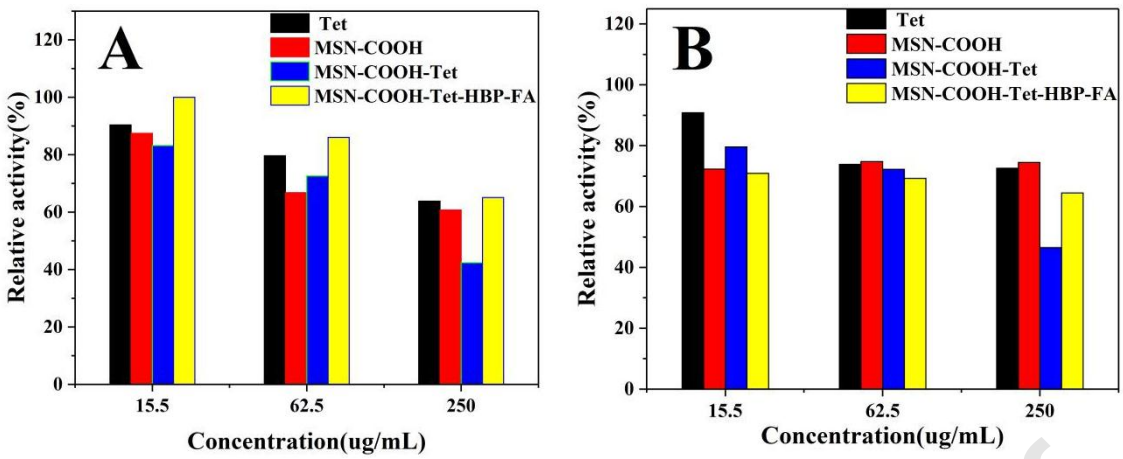

Fig. 11 In vitro cytotoxicity of Tet, MSN-COOH, MSN-COOH-Tet and MSN-COOH-Tet-HBP-FA in Hela cells(A)and A549 cells(B) after incubation for 48 h.

3.4. Cellular Uptake Assay

After FA moiety conjugation, MSN-COOH-Tet-HBP-FA complexes could be internalized by cancer cells due to folate receptor-mediated endocytosis. To visualize intracellular Tet release, the cellular uptake of Tet-loaded nanomparticles was further investigated by confocal laser scanning microscopy (Figure 12, Figure 13). Lyso Tracker lysosomes were labeled with red fluorescent markers and DAPI, respectively. The blue region is the nucleus of cells, green is the fluorescent nanoparticles, and red is the lysosomes in the cytoplasm. It can be seen from the figure that the green fluorescence emitted by the FITC-MSNs is widely distributed in the cytoplasm, indicating that the nanoparticles enter the cytoplasm after being ingested by the cells. The superimposed photographs shows that MSN-COOH has a large number of green bright spots and a small amount of yellow bright spots (the superposition of green MSN-COOH-FITC and red lysosomal highlights) after 24 hours of coculture in both cells, showing significant lysosomal escape. However, the superimposed photos of folic acid-modifiedl MSN-COOH-Tet-HBP-FA showed a large number of yellow bright spots, indicating that nanoparticles were ingested into lysosomes by Hela and A549 cells. The yellow bright spot of

MSN-COOH-Tet-HBP-FA in Hela cells was significantly higher than that of MSN-COOH, suggesting that the cellular uptake of folic acid modified materials may partly benefit from folic acid receptor mediated active uptake[60,61].

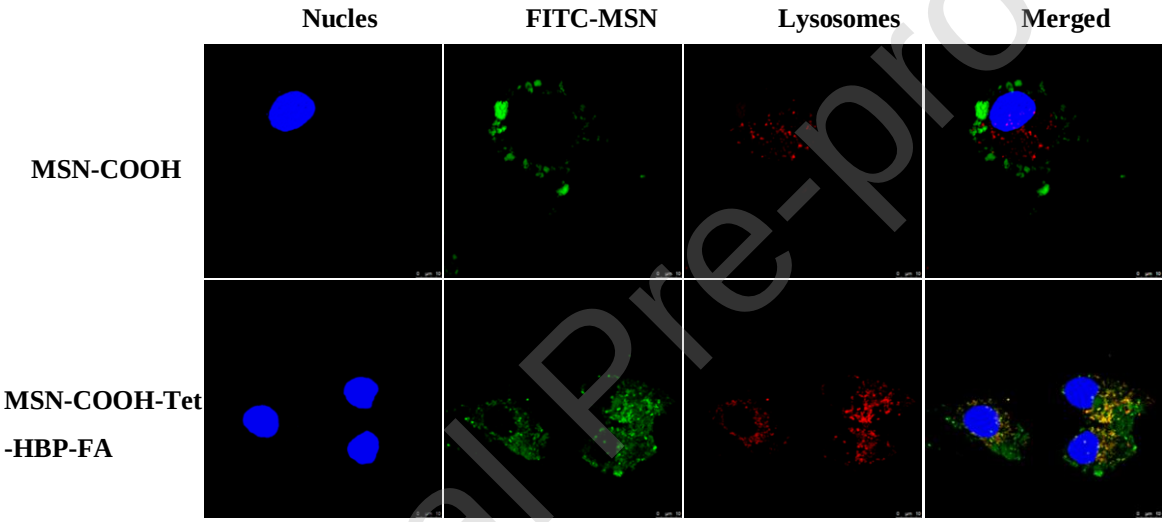

Fig. 12 Confocal laser scanning microscopy (CLSM) of Hela cells after incubation for 24 h with FITC-MSNs of samples MSN-COOH and MSN-COOH-Tet-HBP-FA

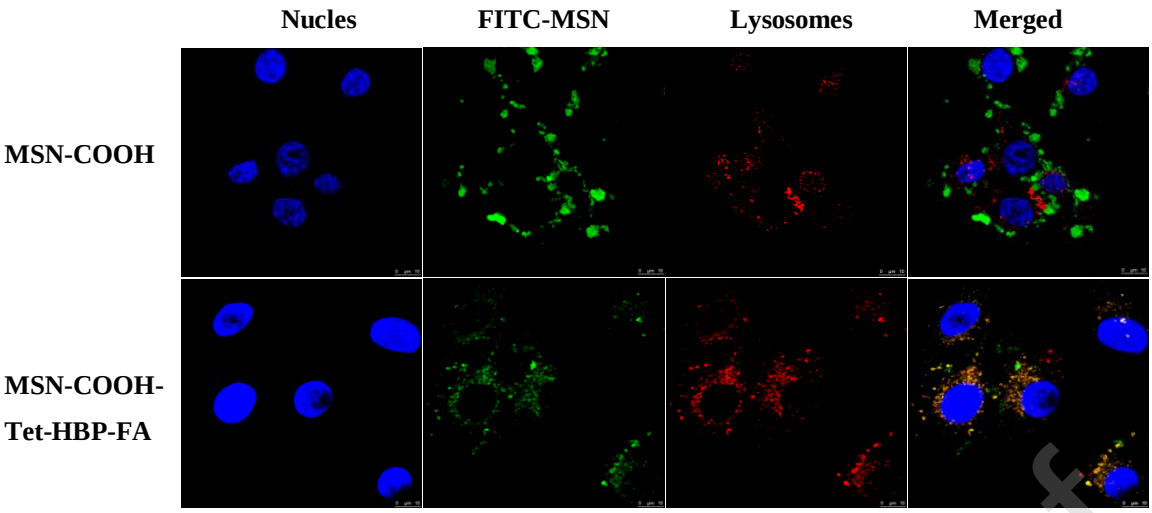

Fig. 13 Confocal laser scanning microscopy (CLSM) of A549 cells after incubation for 24 h with FITC-MSNs of samples MSN-COOH and MSN-COOH-Tet-HBP-FA

4. Conclusions

In summary, multifunctional MSNs (MSN-COOH-Tet-HBP-FA) with particle a size of 130 nm for folic acid-mediated active targeting and pH stimulation response were successfully synthesized as a vector for the delivery of the antitumor drug tetrahexine. The high loading efficiency of tetrandrine (26.86%) was achieved by carboxyl modification and grafting of HBP and folic acid, as well as enhanced toxicity to Hela and A549 cells. Furthermore, the hyperbranched polymer HBP is attached to the outside of the mesopores and encapsulates the drug molecules in the mesopores as a cap, which improves the stability of the carrier material and enables the drug to achieve "zero pre-release" within 20 hours in a normal physiological environment. MSN-COOH-Tet-HBP-FA has good biocompatibility and is taken up into lysosomes of Hela cells and A549 cells, and exhibits folate receptor-mediated active uptake in Hela cells. These results indicated that MSN-COOH-Tet-HBP-FA could be potential carriers for anticancer drug delivery.

Competing Interests

The authors declare no conflicting interests.

Funding

We acknowledge financial support from the Guizhou provincial science and technology department joint fund project (QKHLH[2017]7289) and the talent introduction project of Guizhou University (Gui Da Ren Ji He Zi [2019] 13).

Acknowledgment

We thank Guizhou university test center for characterization of TEM and SEM of materials, and all those who contributed to the study but did not meet the authorship criteria. We thank Enpaper (www.Enpaper.com) for its linguistic assistance during the preparation of this manuscript.

References

[1] J.H. Im, J. Seong, I.J. Lee, J.S. Park, D. S. Yoon, K.S. Kim, W.J. Lee, K. R. Park, Surgery Alone Versus Surgery Followed by Chemotherapy and Radiotherapy in Resected Extrahepatic Bile Duct Cancer: Treatment Outcome Analysis of 336 Patients, Cancer Research and Treatment, 48(2015) 583-595.

[2] S.T. Wang, J.T. Li, Z. Ye, J.L. Li, A.H. Wang, J. Hu, S.Bai, J.Yin, Self-Assembly of Photosensitive and Chemotherapeutic Drugs for Combined Photodynamic-Chemo Cancer Therapy with Real-Time Tracing Property, Colloids and Surfaces A, 574 (2019) 44–51.

[3] A. Armiñán, P.S. Martina, C. Deladriere, J.A.C. Juan, V.R. Sonia, J.V. Maríat, P.L.Antonio, Metabolomics facilitates the discrimination of the specific anti-cancer effects of free- and polymer-conjugated doxorubicin in breast cancer models, Biomaterials, 162 (2018) 144 -153.

[4] T.J. Ji, S.P. Li, Y.L. Zhang, J.Y. Lang, Y.P. Ding, X. Zhao, R.F. Zhao, Y.Y. Li, J. Shi, J.H. Hao, Y. Zhao, G.J. Nie, An MMP-2 responsive liposome integrating anti-fibrosis and chemotherapeutic

drugs for enhanced drug perfusion and efficacy in pancreatic cancer, ACS Appl. Mater. Interfaces, 8(2016) 3438-3445.

[5] X.R. Li, V.M.Garamus, N. Li, Y.B. Gong, Zh. Zhe, Zh.F. Tian, A.H. Zou, Preparation and characterization of a pH-responsive mesoporous silica nanoparticle dual-modified with biopolymers, Colloids and Surfaces A, 548 (2018) 61–69.

[6] H. Li, Y. Jia, H.N. Peng, J.B. Li, Recent developments in dopamine-based materials for cancer diagnosis and therapy, Advances in Colloid and Interface Science, 252 (2018) 1–20.

[7] H. Li, Y.Y. Zhao, Y. Jia, C.T. Qu, J.B. Li, Covalently assembled dopamine nanoparticle as an intrinsic photosensitizer and pH-responsive nanocarrier for potential application in anticancer therapy, Chem. Commun, 55(2019) 15057-15060.

[8] M.Yu, F. Guo, F.P.Tan, N. Li, Dual-targeting nanocarrier system based on thermosensitive liposomes and gold nanorods for cancer thermo-chemotherapy, Journal of Controlled Release, 215(2015) 91-100.

[9] Goncalves M C, Mertins O, Pohlmann A R, et al. M.C.F. Gonçalves, O. Mertins, A.R. Pohlmann, N.P. Silveira, S.S. Guterres, Chitosan coated liposomes as an innovative nanocarrier for drugs, Journal of Biomedical Nanotechnology, 8(2012) 240-250.

[10] A. Pucci, E Locatelli, J. Ponti, C. Uboldi, V. Molinari, M.C. Franchini, Click Chemistry on the Surface of PLGA-b-PEG Polymeric Nanoparticles: A Novel Targetable Fluorescent Imaging Nanocarrier, Journal of Nanoparticle Research, 15(2013) 1-6.

[11] Q. Cheng, L.L. Du, L.W. Meng, S.C.Han, T. Wei, X.X. Wang, Y.D. Wu, X.Y. Song, J.H. Zhou, S.Q Zheng, Y.Y. Huang, X.J. Liang, H.Q. Cao, A.J. Dong, Z.C. Liang, The Promising Nanocarrier for Doxorubicin and siRNA Co-delivery by PDMAEMA-based Amphiphilic Nanomicelles, ACS Appl.

Mater. Interfaces, 8(2016) 4347-4356.

[12] Zhao Z, Gao S, Wang J, et al. Z.X. Zhao, S.Y. Gao, J.C. Wang, C.J. Chen, E.Y. Zhao, W.J. Hou, Q. Feng, L.Y. Gao, X.Y. Liu, L.R. Zhang, Q. Zhang, Self-assembly nanomicelles based on cationic mPEG-PLA-b-Polyarginine (R15) triblock copolymer for siRNA delivery, Biomaterials, 33(2012) 6793-6807.

[13] YanLi, H. He, X.R. Jia, W.L. Lu, J.N. Lou, Y. Wei, A dual-targeting nanocarrier based on poly (amidoamine) dendrimers conjugated with transferrin and tamoxifen for treating brain gliomas,. Biomaterials, 33(2012) 3899-3908.

[14] A.P.Sherje, M. Jadhav, B.R. Dravyakar, D. Kadam, Dendrimers: A versatile nanocarrier for drug delivery and targeting, International Journal of Pharmaceutics, 548(2018) 707-720.

[15] D. Peer, J.M. Karp, S. Hong, O.C. Farokhzad, R. Margalit, R. Langer, Nanocarriers as an emerging platform for cancer therapy, Nature Nanotechnology, 2(2007) 751-760.

[16] Ch. Han, N. Cai, V. Chan, M.M. Liu, X.J. Feng, F.Q. Yu, Enhanced drug delivery, mechanical properties and antimicrobial activities in poly(lactic acid) nanofiber with mesoporous Fe3O4-COOH nanoparticles, Colloids and Surfaces A, 559 (2018) 104–114.

[17] A. Schroeder, D.A. Heller, M.M. Winslow, J.E. Dahlman, G.W. Pratt, R. Langer, T.r Jacks, D.G. Anderson , Treating metastatic cancer with nanotechnology, Nature Reviews Cancer, 12(2011) 39-50.

[18] J.D. Byrne, T. Betancourt, L. Brannonpeppas, Active targeting schemes for nanoparticle systems in cancer therapeutics, Adv Drug Deliv Rev, 60(2008) 1615-1626.

[19] T. Doi, H. Iwata, J. Tsurutani, S. Takahashi, H. Park, C.H. Redfern, K. Shitara, C. Shimizu, H. Taniguchi, T. Iwasa, S. Taira, A.C. Lockhart, J.M. Fisher, T. Jikoh, Y. Fujisaki, C.C. Lee, A.

Yver, K. Tamura, Single agent activity of DS-8201a, a HER2-targeting antibody-drug conjugate, in heavily pretreated HER2 expressing solid tumors, Journal of Clinical Oncology, 35(2017) 108-108.

[20] Liang L, Lin Z, Lin Y, et al. L. Liu, L. Zhang, L. Yang, H. Li, R. Li, J.P. Yu, L.L. Yang, F. Wei, C.H. Yan, Q. Sun, H. Zhao, F. Yang, H. Jin, J. Wang, S.E. Wang, X.B. Ren, Anti-CD47 Antibody as a Targeted Therapeutic Agent for Human Lung Cancer and Cancer Stem Cells, Frontiers in Immunology, 8(2017) 404.

[21] E.E. Kamarulzaman, R. Vanderesse, A.M. Gazzali, B.H. Muriel, C. Boura, C. Frochot, O. Shawkataly, A. Aubry, H.A. Wahab, Molecular modelling, synthesis and biological evaluation of peptide inhibitors as anti-angiogenic agent targeting neuropilin-1 for anticancer application, Journal of Biomolecular Structure & Dynamics, 35(2017) 26-45.

[22] G.Ch. Chen, Y.Sh. Xie, R. Peltier, H.P. Lei, P. Wang, J. Chen, Y. Hu, F. Wang, X. Yao, H.Y. Sun, Peptide-Decorated Gold Nanoparticles as Functional Nano-Capping Agent of Mesoporous Silica Container for Targeting Drug Delivery, ACS Applied Materials & Interfaces, 8(2016) 11204-11209.

[23] A.R. Lavik, F. Zhong, M.J. Chang, E. Greenberg, Y. Choudhary, M.R. Smith, K.S. McColl, J. Pink, Fr.J. Reu, S. Matsuyama, C.W. Distelhorst, A synthetic peptide targeting the BH4 domain of Bcl-2 induces apoptosis in multiple myeloma and follicular lymphoma cells alone or in combination with agents targeting the BH3-binding pocket of Bcl-2 [J]. Oncotarget, 6(2015) 27388-27402.

[24] Predina J D, Newton A D, Connolly C, et al. J.D. Predina, A.D. Newton, C. Connolly, A. Dunbar, M. Baldassari, C. Deshpande, E. CantuIII, J. Stadanlick, S.A. Kularatne, P.S.Low, S. Singhal, Identification of a Folate Receptor-Targeted Near-Infrared Molecular Contrast Agent to Localize Pulmonary Adenocarcinomas, Molecular Therapy, 26(2017) 390-403.

[25] R. Guo, L.L. Li, W.H. Zhao, Y.X. Chen, X.Zh. Wang, Ch.J. Fang, W. Feng, T.L. Zhang, X. Ma, M.

Lu, S.Q. Peng, Ch.H. Yan, The Intracellular Controlled Release from Bioresponsive Mesoporous Silica with Folate as both Targeting and Capping Agent, Nanoscale, 4(2012) 3577-3583.

[26] K.M. Au, A. Satterlee, Y.Z. Min, X. Tian, S.K.Young, J.M.Caster, L.Zh. Zhang, T. Zhang, L. Huang, A.Z.Wang, Folate-targeted pH-responsive calcium zoledronate nanoscale metal-organic frameworks: Turning a bone antiresorptive agent into an anticancer therapeutic, Biomaterials, 82(2016) 178-193.

[27] S. Baek, R.K. Singh, D. Khanal, K.D. Patel, E.J. Lee, K.W. Leong, W. Chrzanowski, H.W. Kim, Smart multifunctional drug delivery towards anticancer therapy harmonized in mesoporous nanoparticles, Nanoscale, 7(2015) 14191–14216.

[28] Sh. Yang, J. Fan, Sh.T.Lin, Y.R. Wang, Ch. Liu, Novel pH-responsive biodegradable organosilica nanoparticles as drug delivery system for cancer therapy, Colloids and Surfaces A, 585 (2020) 124133.

[29] M. Hegazy, P. Zhou, N. Rahoui, G.Y.Wu, N. Taloub, Y.P. Lin, X. Huang, Y.D. Huang, A facile design of smart silica nanocarriers via surface-initiated RAFT polymerization as a dual-stimuli drug release platform, Colloids and Surfaces A, 581 (2019) 123797.

[30] Z.J. Liu, J.H. Shi, Y. Wang, Y. Gan, P. Wan, Facile preparation of pyrenemethyl ester-based nanovalve on mesoporous silica coated upconversion nanoparticle for NIR light-triggered drug release with potential monitoring capability, Colloids and Surfaces A, 568 (2019) 436-444.

[31] B.Y. Niu, Y.X. Zhou, T. Wen, G.L. Quan, V. Singh, X. Pan, Ch.B. Wu, Proper functional modification and optimized adsorption conditions improved the DNA loading capacity of mesoporous silica nanoparticles, Colloids and Surfaces A, 548 (2018) 98-107.

[32] S.P. Hudson, R.F. Padera, R. Langer, D.S. Kohane, The biocompatibility of mesoporous silicates,

Biomaterials, 29(2008) 4045-4055.

[33] J.G. Croissant, Y. Fatieiev, N.M. Khashab, Degradability and Clearance of Silicon, Organosilica, Silsesquioxane, Silica Mixed Oxide, and Mesoporous Silica Nanoparticles, Advanced Materials, 29(2017) 1604634.

[34] D.L. Wang, C.L. Tu, Y. Su, C. Zhang, U. Greiser, X.Y. Zhu, D.Y. Yan , W.X. Wang, Supramolecularly engineered phospholipids constructed bynucleobase molecular recognition: upgraded generation of phos-pholipids for drug delivery, Chemical Science, 6(2015) 3775–3787.

[35] Tao W , Zhang J , Zeng X , et al.W. Tao, J.X. Zhang, X.W. Zeng, D. Liu, G. Liu, X.i Zhu, Y.L. Liu, Q.T. Yu, L.Q. Huang, L. Mei, Blended Nanoparticle System Based on Miscible Structurally Similar Polymers: A Safe, Simple, Targeted, and Surprisingly High Efficiency Vehicle for Cancer Therapy, Advanced Healthcare Materials, 4(2015) 1203-1214.

[36] S. Salmaso, A. Semenzato, P. Caliceti, J. Hoebeke, F. Sonvico, C. Dubernet, P. Couvreur, Specific Antitumor Targetable β-Cyclodextrin−Poly(ethyleneGlycol)−Folic Acid Drug Delivery Bioconjugate, Bioconjugate Chemistry, 15(2004) 997-1004.

[37] A.R. Chowdhuri, T. Singh, S.K. Ghosh, S.K. Sahu, Carbon Dots Embedded Magnetic Nanoparticles @ Chitosan @Metal Organic Framework as a Nanoprobes for pH Sensitive Targeted Anticancer Drug Delivery, ACS Appl. Mater. Interfaces, 8(2016) 16573-16583.

[38] J. Sudimack, R.J. Lee, Targeted drug delivery via the folate receptor, Adv Drug Deliv Rev, 41(2002) 147-162.

[39] F. Porta, G.E.M. Lamers, J. Morrhayim, A. Chatzopoulou, M. Schaaf, H. Dulk, C. Backendorf, J.I. Zink, A. Kros, Folic Acid-Modified Mesoporous Silica Nanoparticles for Cellular and Nuclear Targeted Drug Delivery, Advanced Healthcare Materials, 2(2013) 281-286.

[40] S. Karamipour, M.S. Sadjadi, N. Farhadyar, Fabrication and spectroscopic studies of folic acid-conjugated Fe3O4@Au core–shell for targeted drug delivery application, Spectrochimica Acta Part A: Molecular and Biomolecular Spectroscopy, 148(2015) 146-155.

[41] N. Parker, M.J. Turk, E. Westrick, J.D.Lewis, P.S. Low, C.P. Leamon, Folate receptor expression in carcinomas and normal tissues determined by a quantitative radioligand binding assay, Analytical Biochemistry, 338(2005) 284-293.

[42] C.P. Leamon, J.A. Reddy, Folate-targeted chemotherapy, Advanced Drug Delivery Reviews, 56(2004) 1127-1141.

[43] X.K. Zhang, L.J. Meng, Q.H. Lu, Z.F. Fei, P.J. Dyson, Targeted delivery and controlled release of doxorubicin to cancer cells using modified single wall carbon nanotubes, Biomaterials, 30(2009) 6041-6047.

[44] B. Stella, S. Arpicco, M.T. Peracchia, D. Desmaële, J. Hoebeke, M. Renoir, J.D. Angelo, L. Cattel, P. Couvreur, Design of folic acid-conjugated nanoparticles for drug targeting, Journal of pharmaceutical sciences, 89(2000) 1452-1464.

[45] H.Q. Wang, T. Liu, L. Li, Q. Wang, Ch.R. Yu, X. Liu, W.H. Li, Tetrandrine is a potent cell autophagy agonist via activated intracellular reactive oxygen species, Cell & Bioscience, 5(2015) 4.

[46] L.F. Mei, Y.Ch. Chen, Zh.M. Wang, J. Wang, J.L. Wan, Ch.R. Yu, X. Liu, W.H. Li, Synergistic anti-tumour effects of tetrandrine and chloroquine combination therapy in human cancer: a potential antagonistic role for p21, British Journal of Pharmacology, 172(2015) 2232-2245.

[47] Man Y, Ting L, Yicheng C, et al.M. Yu, T. Liu, Y.Ch. Chen, Y.F. Li, W.H. Li, Combination therapy with protein kinase inhibitor H89 and Tetrandrine elicits enhanced synergistic antitumor efficacy, Journal of Experimental & Clinical Cancer Research, 37(2018) 114.

[48] F. Zhang, Y.Y. Chen, H. Lin, Y.H. Lu, Synthesis of an amino-terminated hyperbranched polymer and its application in reactive dyeing on cotton as a salt-free dyeing auxiliary, Coloration Technology, 123(2007) 351–357.

[49] A.L.P. Silva, K.S. Sousa, A.F.S. Germano, V.V. Oliveira, J.G.P. Espínola, M.G. Fonseca, C. Airoldi, T. Arakaki, L.N.H. Arakaki, A new organofunctionalized silica containing thioglycolic acid incorporated for divalent cations removal-A thermodyamic cation/basic center interaction, Colloids and Surfaces A, 332(2009) 144-149.

[50] Sinha A , Basiruddin S , Chakraborty A , et al.A. Sinha, S.K. Basiruddin, A. Chakraborty, N.R. Jana, β-Cyclodextrin Functionalized Magnetic Mesoporous Silica Colloid for Cholesterol Separation, ACS Applied Materials & Interfaces, 7(20152) 1340-1347.

[51] J. Soleymani, M. Hasanzadeh, M. H. Somi, N. Shadjou, A. Jouyban, Probing the Specific Binding of Folic Acid to Folate Receptor using Amino-functionalized Mesoporous Silica Nanoparticles for Differentiation of MCF 7 Tumoral Cells from MCF 10A, Biosensors and Bioelectronics, 115(2018) 61-69.

[52] W.J. Xu, J. Rytkönen, S. Rönkkö, T. Nissinen, T. Kinnunen, M. Suvanto, A. Närvänen, V.P. Lehto, A Nanostopper Approach To Selectively Engineer the Surfaces of Mesoporous Silicon, Chemistry of Materials, 26(2014) 6734-6742.

[53] Y.S. Lin , C.L. Haynes, Impacts of Mesoporous Silica Nanoparticle Size, Pore Ordering, and Pore Integrity on Hemolytic Activity, J. Am. Chem. Soc. 132(2010) 4834-4842.

[54] Vallet-Regi M, Ramila A, Del Real R P, et al.M.V. Regi, A. Rámila, R.P. Real, J.P. Pariente, A new property of MCM-41: drug delivery system, Chemistry of Materials, 13 (2001) 308-311.

[55] C.P. Jaroniec, M. Kruk, M. Jaroniec, A. Sayari, Tailoring surface and structural properties of

MCM-41 silicas by bonding organosilanes, J. Phys. Chem. B, 102(1998) 5503–5510.

[56] N.K. Mal, M. Fujiwara, Y. Tanaka, T. Taguchi, M. Matsukata, Photo-switched storage and release of guest molecules in the pore void of coumarin-modifed MCM-41, Chemistry of Materials, 15(2003) 3385–3394.

[57] R. Chen, L. Wang, Synthesis of an amphiphilic hyperbranched polymer as a novel pH-sensitive drug carrier, Rsc Advances, 5(2015) 20155-20159.

[58] Z.B. Li, E.Y. Ye, David, R. Lakshminarayanan, X.J. Loh, Recent Advances of Using Hybrid Nanocarriers in Remotely Controlled Therapeutic Delivery, Small, 12(2016) 4782-4806.

[59] J. Pushpamalar, A.K. Veeramachineni, C. Owh, X.J. Loh, Biodegradable Polysaccharides for Controlled Drug Delivery, Chempluschem, 81(2016) 504-514.

[60] Lopez V, Villegas M R, Rodríguez, Veronica, et al.V. López, M.R.ío Villegas, V. Rodríguez, G. Villaverde, D. Lozano, A. Baeza, M.V.Regí, Janus mesoporous silica nanoparticles for dual-targeting for tumoral cells and mitochondria, ACS Appl. Mater. Interfaces, 9(2017) 26697-26706.

[61] L. Maggini, I. Cabrera, A. R. Carretero, E.A. Prasetyanto, E. Robinet, L.D. Cola, Breakable mesoporous silica nanoparticles for targeted drug delivery, Nanoscale, 8(2016) 7240-7247 .